Improving zero-mode waveguide structure for enhancing signal-to-noise ratio of real-time single-molecule fluorescence imaging: A computational study

Takashi Tanii,* Rena Akahori, Shun Higano, and Kotaro Okubo
Faculty of Science and Engineering, Waseda University, 3-4-1 Ohkubo, Shinjuku, Tokyo 169-8555, Japan

Hideaki Yamamoto
Waseda Institute for Advanced Study, Waseda University, 1-6-1 Nishiwaseda, Shinjuku, Tokyo 169-8050, Japan

Taro Ueno and Takashi Funatsu
Graduate School of Pharmaceutical Sciences, The University of Tokyo, 7-3-1 Hongo, Bunkyo, Tokyo 113-0033, Japan
(Received 8 May 2013; published 30 July 2013)

We investigated the signal-to-noise ratio (S/N) of real-time single-molecule fluorescence imaging (SMFI) using zero-mode waveguides (ZMWs). The excitation light and the fluorescence propagating from a molecule in the ZMW were analyzed by computational optics simulation. The dependence of the S/N on the ZMW structure was investigated with the diameter and etching depth as the simulation parameters. We found that the SMFI using a conventional ZMW was near the critical level for detecting binding and dissociation events. We show that etching the glass surface of the ZMW by 60 nm enhances the S/N six times the conventional nonetched ZMWs. The enhanced S/N improves the temporal resolution of the SMFI at physiological concentrations.

DOI: 10.1103/PhysRevE.88.012727 PACS number(s): 87.80.Nj

I. INTRODUCTION

Single-molecule fluorescence imaging (SMFI) of a weak ligand-enzyme interaction at physiological concentrations requires confinement of excitation light within an extremely small volume [1]. To fluorescently identify an enzyme-bound ligand among the unity of nonbinding ligands in solution, the excitation light must be irradiated to the bound ligand like a spotlight. Such a small excitation volume can be achieved by scanning near-field optical microscopy [2], Förster resonance energy transfer [3], or zero-mode waveguides (ZMWs) [4,5]. Among the methods, the ZMW is advantageous in terms of ultrasmall excitation volume (∼zeptoliter), real-time detection, and parallel analysis. So far, real-time sequencing of deoxyribonucleic acid (DNA) [6,7] or amino acid [8], real-time imaging of protein-protein interaction [9–11], and live-cell imaging of membrane proteins [12,13] have been demonstrated using ZMWs.

The ZMW is a subwavelength nanohole in a thin metal film on a glass coverslip [Fig. 1(a)]. Since the nanohole diameter is smaller than the excitation wavelength, the excitation light is confined within the nanohole where an enzyme of interest is immobilized [Fig. 1(b)]. The principle of real-time SMFI is as follows. Most dye-labeled ligands undergo Brownian motion in the solution, and they never emit fluorescence outside the nanohole. The ligands enter and exit the nanohole randomly. The ligand emits fluorescence if it enters the nanohole, but the fluorescence intensity is still weak because the excitation volume is sufficiently small as compared to the ligand concentration: Namely, the time-averaged number of ligands within the excitation volume is much less than 1. In contrast, the ligand emits comparatively strong fluorescence when it is bound to the immobilized enzyme. As a result, the fluorescence from an enzyme-bound ligand ("signal") is superimposed onto the fluorescence from free ligands ("background"), thus, the binding and dissociation can be measured as the temporal alternation in the fluorescence intensity.

The background fluorescence intensity fluctuates temporally in accordance with the entrance and exit of the ligands. As shown in Fig. 1(c), the temporal fluctuation gives rise to noise because the randomly fluctuating background fluorescence overlaps the signal fluorescence that represents the binding events. This mixing makes it difficult to distinguish the binding events when the signal-to-noise ratio (S/N) is low. In the case of real-time single-DNA sequencing, missing a binding event leads to a sequencing error [6]. For the analysis of ligand-enzyme interaction kinetics, binding time needs to be measured precisely [10]. Since the background intensity depends on the excitation volume [4], the feasibility of SMFI needs to be examined from the viewpoint of the S/N.

Recently, we found that etching the glass surface at the nanohole base dramatically enhances the signal intensity [9]. The results suggest that the S/N can be enhanced by optimizing the ZMW structure, such as the etching depth. However, it is still unclear whether the etching contributes to S/N enhancement because, at least, the etching increases the excitation volume and, hence, the background intensity. Since the background intensity can be reduced by decreasing the nanohole diameter, both the etching depth and the nanohole diameter need to be taken into account in the evaluation of the S/N.

To investigate the dependence of the S/N on the ZMW structure and to provide theoretical background for the real-time SMFI, we analyzed the intensity of single-molecule fluorescence in ZMWs by three-dimensional computational optics simulation. Both the signal fluorescence intensity from an enzyme-bound ligand and the background fluorescence intensity from free ligands within the excitation volume were calculated. By comparing the signal intensity with the noise intensity, we evaluated the critical concentration at which

*tanii@waseda.jp

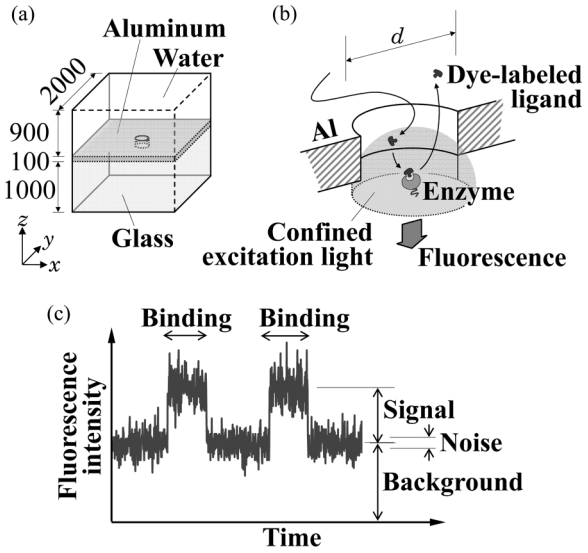

FIG. 1. Schematics of real-time SMFI using ZMW. (a) Geometry of the computational optics simulation model. (b) The binding and dissociation between a dye-labeled ligand and an enzyme immobilized on the nanohole base. (c) Fluorescence signal detected in a ZMW. In the trace shown here, the signal intensity is sufficiently high as compared to the noise intensity ($S = 5\sigma$).

the direct observation of binding-dissociation events between a ligand and an enzyme is feasible. From this simulation, we derive the ZMW structure suitable for real-time SMFI at physiological concentrations.

II. COMPUTATIONAL OPTICS SIMULATION

A finite-element time domain simulation for electromagnetic wave propagation problems was performed using the EMFLEX code (Weidlinger Associates, Inc.) [14]. Figure 1(a) shows a schematic of the simulation model which encompasses a 2-μm cube. A glass substrate, an aluminum film (thickness: 100 nm), and water were aligned in the z direction, and a nanohole was placed in the center. The grid mesh was set to be fine (3-nm intervals) in the vicinity of the nanohole and coarse (17-nm intervals) in the peripheral region. The electric permittivity of the glass, aluminum, and water were set to be 2.12, -5.01×10^{-10}, and 1.78 F m^{-1}, respectively. The electric conductivity of the aluminum was set to be -5.01×10^{5} S m^{-1} [15].

Theoretically, the fluorescence intensity from a ligand at position $\boldsymbol{r}$ is given by $F(\boldsymbol{r}) = I(\boldsymbol{r})P(\boldsymbol{r})Q(\boldsymbol{r})$, where $I(\boldsymbol{r})$ is the intensity of excitation light, $P(\boldsymbol{r})$ is the detection efficiency (or dipole coupling efficiency [4]), and $Q(\boldsymbol{r})$ is the quantum yield of the fluorescent dye [16–18]. Because $I(\boldsymbol{r})$ and $P(\boldsymbol{r})$ depend strongly on the depth z at which the ligand is fluorescently excited and independent of x and y at a constant depth, we ignore the in-plane distributions of $I(\boldsymbol{r})$ and $P(\boldsymbol{r})$ as is conventionally done [4]. Also, we assume a constant quantum yield of $Q(\boldsymbol{r}) = 1$. On the basis of the above assumptions, the fluorescent intensity is approximated as $F(z) = I(z)P(z)$, where z is the depth at which the ligand is fluorescently excited. For convenience, the z axis is defined as the central axis of the nanohole.

The procedure for calculating $F(z)$ is as follows. The first simulation was performed to obtain the distribution of excitation light intensity $I(z)$. In this simulation, the ZMW with a given diameter and an etching depth was irradiated with a circularly polarized light at a wavelength of 635 nm from the basal plane of the simulation model. The electromagnetic field vector at each grid point was calculated by solving the Maxwell equations in the time domain based on the finite-element approach. The time domain calculation was carried out until a steady state was achieved. We extracted the depth distribution of the electric field vector along the z axis, and $I(z)$ was obtained as a square of the electric field vector. The second simulation was performed to obtain the detection efficiency $P(z)$. The second simulation was carried out separately from the first simulation. Here, a pointlike source of light was set in the ZMW, and the wave propagating from this pointlike source of light was simulated. Excitation light was not introduced, and the pointlike light source was the only light source in the second simulation. The diameter of the pointlike light source was set to be 24 nm, and the inner boundary condition was defined so as to emit a diffusive light at a wavelength of 670 nm. The emission power was fixed in the simulation. Thus, the pointlike source of light represented fluorescence emitted from a ligand within the nanohole at a fixed excitation intensity. Since the fluorescence propagating back into the glass substrate is captured by the photodetector, the intensity of light at the whole outer boundary of the glass region of the simulation model was regarded as $P(z)$. The simulation for $P(z)$ was performed every time the position of the pointlike light source was changed along the z axis. Also, the simulation was performed three times for the same depth z, each with the pointlike source of light polarized in the x, y, or z direction. This is because the ligand moves freely in the waveguide, hence, the orientation of the fluorescent dye at z also fluctuates randomly. We averaged three $P(z)$ values obtained from the pointlike light source polarized in the x, y, or z direction. Finally, $F(z)$ was calculated by multiplying $I(z)$ and the averaged $P(z)$.

The background fluorescence intensity from free ligands within the excitation volume was estimated as $B = CV_{\mathrm{eff}}$, where C is the concentration of fluorescently labeled ligands and V_{eff} is the effective excitation volume. As reported previously [4,19], the effective excitation volume can be calculated as $V_{\mathrm{eff}} = \pi(\frac{d}{2})^2 \frac{[\int F(z)dz]^2}{\int F^2(z)dz}$. To evaluate V_{eff}, we divided the nanohole volume into j slabs in the z direction [see the inset of Fig. 3(c)] and calculated the discrete $F(z_j)$ values. This is because $P(z)$ was calculated by placing a pointlike source of light in each j slab, hence, $P(z)$ was not obtained as a continuous function but as discrete values. Thus, the background fluorescence intensity was calculated as $B = C\pi(\frac{d}{2})^2 \sum_j \frac{[F(z_j)\Delta z]^2}{F^2(z_j)\Delta z}$.

III. RESULTS AND DISCUSSION

Achieving a high S/N is a requirement to measure binding and dissociation between a ligand and an enzyme fluorescently. To examine the S/N, both the signal intensity and the noise intensity must be evaluated. Fluorescence from a ligand bound to an enzyme in the ZMW determines the signal intensity (S).

We assume that the enzyme is immobilized in the center of the nanohole base and the ligand emits fluorescence in the same position. Thus, S is calculated as $S = F(z_0) = I(z_0)P(z_0)$, where z_0 is the depth of the nanohole base.

Meanwhile, the magnitude of fluctuation in the fluorescence from free ligands determines the noise intensity (N). The number of ligands found in the excitation volume in a unit time obeys Poisson distribution; hence, the number of photons that is emitted from the free ligands in a unit time and, consequently, that reaches a detector obeys Poisson distribution. The mean value of this Poisson distribution is equivalent to B. Since mean and dispersion are equal in a Poisson distribution, the root mean square deviation is given by $\sigma = \sqrt{B}$. Generally, root mean square noise N is defined to be equivalent to σ [20,21], therefore, N is calculated as $N = \sqrt{B}$.

Figure 2 shows the dependence of the excitation intensity on the ZMW structure. As shown in Figs. 2(a) and 2(b), the excitation volume decreases markedly with decreasing nanohole diameter. This indicates that N diminishes with decreasing nanohole diameter because, at a constant ligand concentration, $N = \sqrt{CV_{\text{eff}}}$. Meanwhile, the excitation intensity also decreases with decreasing diameter. As shown in Fig. 2(c), $I(0)$ decreases 2.9 times as the diameter of conventional nonetched waveguide decreases from 150 to 50 nm. This decrease in the excitation intensity leads to a decrease in the fluorescence intensity from the enzyme-bound ligand because the signal intensity of a conventional nonetched waveguide is given by $S = I(0)P(0)$. These results indicate that miniaturizing the nanohole diameter is not effective for enhancing the S/N because the decrease in N is counterbalanced by the decrease in S.

The simulation results show, however, that etching the glass surface of the nanohole base is effective for increasing S. As shown in Fig. 2(c), the peak of the excitation light is located at a depth of a quarter of a wavelength inside the glass because the excitation light is reflected by the aluminum film and forms a standing wave in the glass (for more details, see the Appendix). As the result, the excitation intensity at $z = -60$ nm [$I(-60)$] is 4.1 times higher than that at the bottom of the conventional nonetched waveguide [$I(0)$]. Furthermore, as shown in Fig. 3 , the etching of the waveguide base also enhances the detection efficiency. The fluorescence from the ligand in the etched region propagates freely to the detector [Fig. 3(a)], whereas, the fluorescence does not reach the detector efficiently when

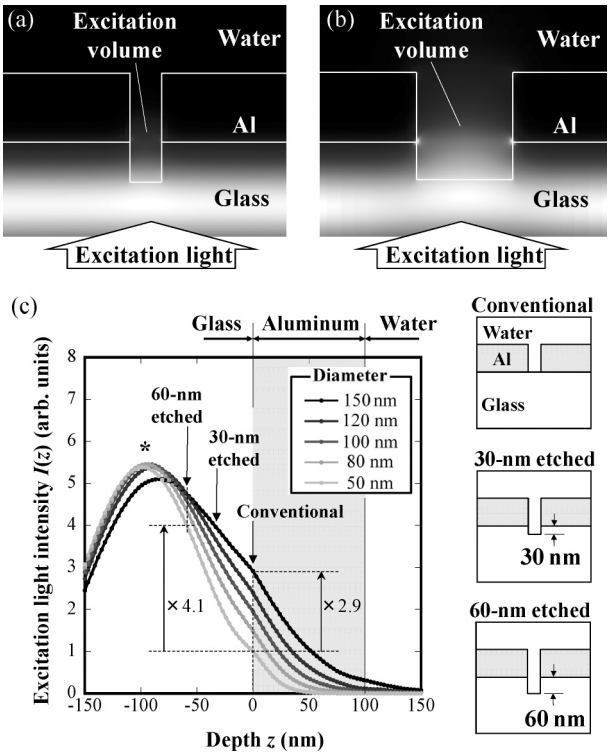

FIG. 2. Evaluation of excitation intensity $I(z)$. Distribution of the excitation light in the vicinity of the ZMW for a diameter of (a) 50 and (b) 150 nm. (c) Excitation intensity profile along the central axis of the nanohole. Since the difference between the $I(z)$ profile for the conventional waveguide and that for the etched waveguide is negligible, a single representative curve is depicted for each diameter. In the vicinity of the aluminum-glass interface, the excitation light forms a standing wave, the first peak of which is depicted with an ∗.

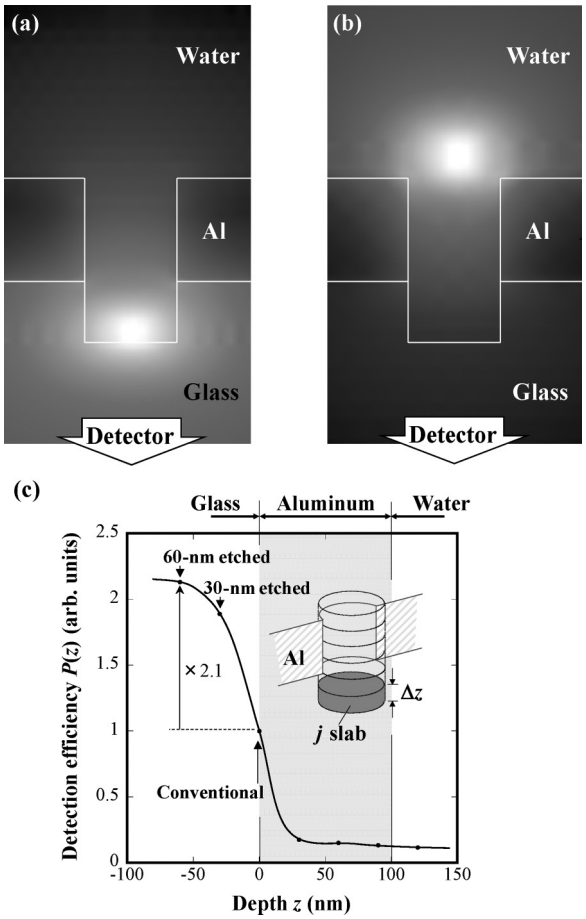

FIG. 3. Evaluation of detection efficiency $P(z)$. (a) Wave propagation from a pointlike source of light placed at the basal plane of a 60-nm-etched waveguide (diameter: 100 nm), and (b) wave propagation from a pointlike source of light placed further from the glass. (c) Detection efficiency $P(z)$. Since the simulation results revealed little difference in the $P(z)$ when the nanohole diameter was changed from 50 to 150 nm, only one line representing the detection efficiency of a 100-nm-diameter nanohole is shown.

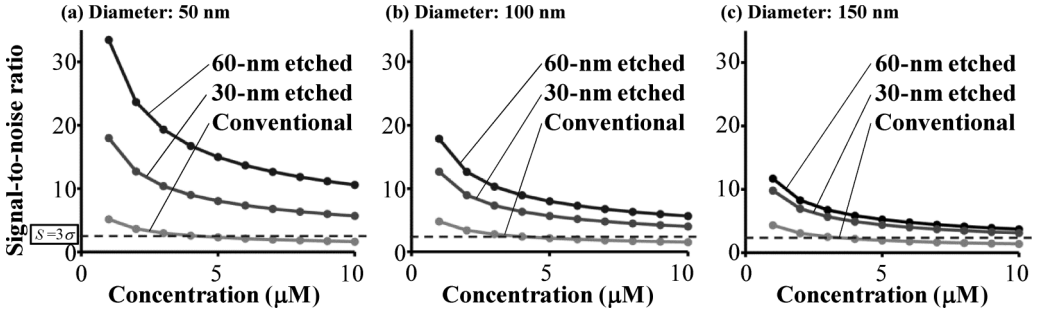

FIG. 4. The S/N in the SMFI with ZMWs of different diameters and etching depths. The S/N was calculated as $F(z_0)/\sqrt{B}$. Dotted lines indicate the detection limit ($S = 3\sigma$) for real-time SMFI.

the ligand is placed further from the glass surface [Fig. 3(b)]. Even in the etched region ($z < 0$), the detection efficiency increases with increasing etching depth [Fig. 3(c)]. As the result, the detection efficiency of the 60-nm-etched waveguide [$P(-60)$] is 2.1 times higher than that of the conventional nonetched waveguide [$P(0)$].

The etching of the glass surface increases not only the signal intensity, but also the excitation volume, resulting in the increase in the noise intensity. In this sense, the effect of the etching must be evaluated in terms of the S/N. Figure 4 shows the dependence of the S/N on the ZMW structure. As shown in Figs. 4(a)–4(c), the S/N of the conventional nonetched waveguide is almost constant, independent of the nanohole diameter. This is because, as discussed above, the decrease in the excitation volume and, hence, the decrease in N are counterbalanced by the decrease in S. In contrast, the S/N of the etched waveguide increases with decreasing nanohole diameter. This indicates that, although the etching increases the excitation volume, the increase in S exceeds the increase in N. The reason is as follows. The excitation volume is proportional to the etching depth and to the square diameter. Accordingly, N is proportional to the square root of the etching depth and to the diameter. This indicates that the increase in N due to etching can be compensated by decreasing the diameter. Meanwhile, S is enhanced by the etching because of the increase in both the excitation intensity and the detection efficiency. As a result, the increase in the S/N by the etching is obvious in the smaller waveguides. The S/N of 60-nm-etched waveguide is more than six times higher than that of the conventional nonetched waveguide.

Microscopy analysis, in general, requires signal intensity greater than 3σ [18]. It follows that real-time SMFI using ZMWs requires the condition of $S/N > 3$. Under this condition, the probability of missing a binding event is less than 0.5%. This detection limit is depicted with dotted lines in Fig. 4. It is obvious that the S/N of the conventional nonetched waveguide is comparable to the detection limit, whereas, the etched waveguide exceeds the detection limit at a concentration as high as 10 μM.

Enzymes are sometimes immobilized on a glass surface with bifunctional cross-linkers to maintain their biological activity [22,23]. When long linkers are used, the S/N decreases because the enzyme is placed apart from the glass surface ($z > 0$). In addition, placing organic dye molecules in the vicinity of the metal clad causes a decrease in the fluorescence intensity due to charge transfer. Therefore, it is advantageous to etch the glass surface and to immobilize the enzyme in the etched region.

IV. CONCLUSION

To investigate the feasibility of real-time SMFI using ZMWs, we conducted a series of computational optics simulations and evaluated the dependence of the S/N on the ZMW structure. The etching of the nanohole base increases both the excitation intensity and the detection efficiency. Although the noise intensity is simultaneously enhanced by the etching, the increase in the signal intensity exceeds that in the noise intensity, resulting in the marked increase in the S/N. As a result, the S/N of 60-nm-etched waveguide 50 nm in the diameter greatly exceeds the critical level for the real-time SMFI. We conclude from the computational optics simulation that the etched waveguide is advantageous for visualizing binding and dissociation events clearly in real time.

ACKNOWLEDGMENTS

This work was supported by a Grant-in-Aid for Basic Research (B) (Grant No. 20310069) from the Ministry of Education, Culture, Sports, Science and Technology, Japan and by the Consolidated Research Institute for Advanced Science and Medical Care founded by the Ministry of Education, Culture, Sports, Science and Technology, Japan.

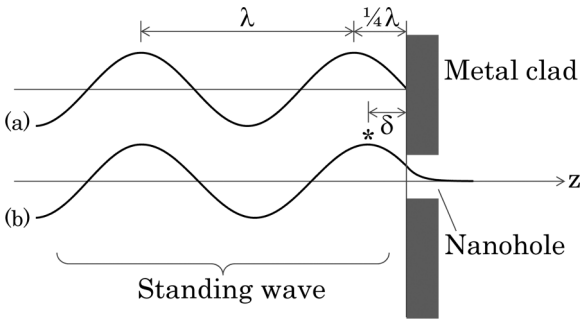

FIG. 5. Standing waves of the incident excitation light formed in the vicinity of a ZMW. (a) The incident light is reflected directly by the metal. (b) The incident light penetrates into the nanohole. The first peak of the standing wave is depicted with an $*$.

APPENDIX: FORMATION OF A STANDING WAVE

Because no propagating modes exist in a subwavelength nanohole, the metal film with nanoholes totally reflects the incident excitation light. Ideally, the metal layer on the glass substrate creates a boundary condition that the light intensity vanishes at the metal-glass interface. This reflection induces the formation of a standing wave in the glass, and the point of the maximum intensity is located at a depth that is a quarter of a wavelength inside the glass [see wave (a) in Fig. 5]. Such a standing wave is also formed when the nanohole is directly illuminated with the excitation light [see wave (b) in Fig. 5]. However, because the excitation light penetrates into the nanohole, the location of the peak shifts toward the interface. The distance δ depends on the depth of penetration to the nanohole. Because, as shown in Fig. 2(c), the penetration depth increases with increasing nanohole diameter, δ decreases with increasing nanohole diameter. The simulation results showed that, when the ZMW is illuminated with an excitation light at the wavelength (λ) of 635 nm, δ is approximately 99 nm for the 150-nm-diameter ZMW, 96 nm for the 120-nm-diameter ZMW, 93 nm for the 100-nm-diameter ZMW, 90 nm for the 80-nm-diameter ZMW, and 84 nm for the 50-nm-diameter ZMW.

[1] T. A. Laurence and S. Weiss, Science **299**, 667 (2003).

[2] A. Lewis, M. Isaacson, A. Harootunian, and A. Muray, Ultramicroscopy **13**, 227 (1984).

[3] M. Sugawa, S. Nishikawa, A. H. Iwane, V. Biju, and T. Yanagida, Small **6**, 346 (2010).

[4] M. J. Levene, J. Korlach, S. W. Turner, M. Foquet, H. G. Craighead, and W. W. Webb, Science **299**, 682 (2003).

[5] C. Genet and T. W. Ebbesen, Nature (London) **445**, 39 (2007).

[6] J. Eid *et al*., Science **323**, 133 (2009).

[7] B. A. Flusberg, D. R. Webster, J. H. Lee, K. J. Travers, E. C. Olivares, T. A. Clark, J. Korlach, and S. W. Turner, Nat. Methods **7**, 461 (2010).

[8] S. Uemura, C. E. Aitken, J. Korlach, B. A. Flusberg, S. W. Turner, and J. D. Puglisi, Nature (London) **464**, 1012 (2010).

[9] T. Miyake, T. Tanii, H. Sonobe, R. Akahori, N. Shimamoto, T. Ueno, T. Funatsu, and I. Ohdomari, Anal. Chem. **80**, 6018 (2008).

[10] M. Suzuki, T. Ueno, R. Iizuka, T. Miura, T. Zako, R. Akahori, T. Miyake, N. Shimamoto, M. Aoki, T. Tanii, I. Ohdomari, and T. Funatsu, J. Biol. Chem. **283**, 23931 (2008).

[11] T. Sameshima, R. Iizuka, T. Ueno, J. Wada, M. Aoki, N. Shimamoto, I. Ohdomari, T. Tanii, and T. Funatsu, J. Biol. Chem. **285**, 285 (2010).

[12] K. T. Samiee, J. M. Moran-Mirabal, Y. K. Cheung, and H. G. Craighead, Biophys. J. **90**, 3288 (2006).

[13] C. I. Richards, K. Luong, R. Srinivasan, S. W. Turner, D. A. Dougherty, J. Korlach, and H. A. Lester, Nano Lett. **12**, 3690 (2012).

[14] J. Mould and D. K. Vaughan, *EMFlex User's Manual* (Weidlinger Associates, New York, 2001), p. 1-J.6.

[15] D. Smith, E. Shiles, and M. Inokuti, *Handbook of Optical Constants of Solids* (Academic, London, 1998), Vol. 1.

[16] C. Zander, J. Enderlein, and R. A. Keller, *Single Molecule Detection in Solution Method and Applications*, 1st ed. (Wiley-VCH, New York, 2002).

[17] D. Axelrod, T. P. Burghardt, and N. L. Thompson, Annu. Rev. Biophys. Bioeng. **13**, 247 (1984).

[18] W. E. Moerner and D. P. Fromm, Rev. Sci. Instrum. **74**, 3597 (2003).

[19] C. Xu and W. W. Webb, in *Topics in Fluorescence Spectroscopy*, edited by J. R. Lakowicz, Vol. 5 (Plenum, New York, 1997), p. 471.

[20] T. Kues, R. Peters, and U. Kubitscheck, Biophys. J. **80**, 2954 (2001).

[21] U. Kubitscheck, T. Kues, and R. Peters, Methods Enzymol. **307**, 207 (1999).

[22] M. Foquet, K. T. Samiee, X. Kong, B. P. Chauduri, P. M. Lundquist, S. W. Turner, J. Freudenthal, and D. B. Roitman, J. Appl. Phys. **103**, 034301 (2008).

[23] J. Wada, S. Ryu, Y. Asano, T. Ueno, T. Funatsu, T. Yukawa, J. Mizuno, and T. Tanii, Jpn. J. Appl. Phys. **50**, 06GK07 (2011).